Improved photoluminescence and afterglow of $CaTiO_3:Pr^{3+}$ by ammonia treatment

Yoon, Songhak; Otal, Eugenio H.; Maegli, Alexandra E.; Karvonen, Lassi; Matam, Santhosh K.; Riegg, Stefan; Ebbinghaus, Stefan G.; Fallas Chinchilla, Juan Carlos; Hagemann, Hans-Rudolf; Walfort, Bernhard; Pokrant, Simone; Weidenkaff, Anke

How to cite

YOON, Songhak et al. Improved photoluminescence and afterglow of $CaTiO_3:Pr^{3+}$ by ammonia treatment. In: Optical materials express, 2013, vol. 3, n° 2, p. 248. doi: 10.1364/OME.3.000248

This publication URL: https://archive-ouverte.unige.ch/unige:26402
Publication DOI: 10.1364/OME.3.000248

Improved photoluminescence and afterglow of $CaTiO_3:Pr^{3+}$ by ammonia treatment

Songhak Yoon,[1] Eugenio H. Otal,[1] Alexandra E. Maegli,[1] Lassi Karvonen,[1] Santhosh K. Matam,[1] Stefan Riegg,[2] Stefan G. Ebbinghaus,[3] Juan C. Fallas,[4] Hans Hagemann,[4] Bernhard Walfort,[5] Simone Pokrant,[1] and Anke Weidenkaff[1,*]

[1]*Laboratory for Solid State Chemistry and Catalysis, Empa - Swiss Federal Laboratories for Materials Science and Technology, Ueberlandstrasse 129, CH-8600, Dübendorf, Switzerland*
[2]*Lehrstuhl für Experimentalphysik 5, EKM, Universität Augsburg, Universitätsstraße 1, 86135 Augsburg, Germany*
[3]*Institut für Chemie, Martin-Luther Universität Halle-Wittenberg, Kurt-Mothes-Straße 2, 06120 Halle/Saale, Germany*
[4]*Département de Chimie Physique, Univ. de Genève, 30, quai E. Ansermet, CH-1211 Geneva 4, Switzerland*
[5]*LumiNova AG, Speicherstrasse 60A, CH-9053, Teufen, Switzerland*
**anke.weidenkaff@empa.ch*

Abstract: The phosphor $CaTiO_3:Pr^{3+}$ was synthesized via a solid-state reaction in combination with a subsequent annealing under flowing NH_3. Comparatively large off-center displacements of Ti in the TiO_6 octahedra were confirmed for as-synthesized $CaTiO_3:Pr^3$ by XANES. Raman spectroscopy showed that the local crystal structure becomes highly symmetric when the powders are ammonolyzed at 400 °C. Rietveld refinement of powder X-ray diffraction data revealed that the samples ammonolyzed at 400 °C have the smallest lattice strain and at the same time the largest average Ti-O-Ti angles were obtained. The samples ammonolyzed at 400 °C also showed the smallest mass loss during the thermal re-oxidation in thermogravimetric analysis (TGA). Enhanced photolumincescence brightness and an improved decay curve as well as the highest reflectance were obtained for the samples ammonolyzed at 400 °C. The improved photoluminescence and afterglow by NH_3 treatment are explained as a result of the reduced concentration of oxygen excesses with simultaneous relaxation of the lattice strain.

OCIS codes: (160.2540) Fluorescent and luminescent materials; (160.4760) Optical properties; (160.5690) Rare-earth-doped materials.

References and links

1. J. Y. Tsao, H. D. Saunders, J. R. Creighton, M. E. Coltrin, and J. A. Simmons, "Solid-state lighting: an energy-economics perspective," J. Phys. D Appl. Phys. **43**(35), 354001 (2010).
2. T. Matsuzawa, Y. Aoki, N. Takeuchi, and Y. Murayama, "New long phosphorescent phosphor with high brightness, $SrAl_2O_4:Eu^{2+},Dy^{3+}$," J. Electrochem. Soc. **143**(8), 2670–2673 (1996).
3. B. M. J. Smets, "Phosphors based on rare-earths, a new era in fluorescent lighting," Mater. Chem. Phys. **16**(3–4), 283–299 (1987).
4. Y. H. Lin, Z. L. Tang, Z. T. Zhang, and C. W. Nan, "Anomalous luminescence in $Sr_4Al_{14}O_{25}$:Eu, Dy phosphors," Appl. Phys. Lett. **81**(6), 996–998 (2002).
5. X. D. Lü, W. G. Shu, Q. Fang, Q. M. Yu, and X. Q. Xiong, "Roles of doping ions in persistent luminescence of $SrAl_2O_4:Eu^{2+}$, Re^{3+} phosphors," J. Mater. Sci. **42**(15), 6240–6245 (2007).
6. A. Vecht, D. W. Smith, S. S. Chadha, C. S. Gibbons, J. Koh, and D. Morton, "New electron excited light-emitting materials," J. Vac. Sci. Technol. B **12**(2), 781–784 (1994).
7. P. T. Diallo, P. Boutinaud, R. Mahiou, and J. C. Cousseins, "Red luminescence in Pr^{3+}-doped calcium titanates," Phys. Status. Solidi A **160**(1), 255–263 (1997).
8. D. Haranath, A. F. Khan, and H. Chander, "Bright red luminescence and energy transfer of Pr^{3+}-doped $(Ca,Zn)TiO_3$ phosphor for long decay applications," J. Phys. D Appl. Phys. **39**(23), 4956–4960 (2006).
9. E. Pinel, P. Boutinaud, and R. Mahiou, "What makes the luminescence of Pr^{3+} different in $CaTiO_3$ and $CaZrO_3$?" J. Alloy. Comp. **380**(1–2), 225–229 (2004).
10. W. Jia, D. Jia, T. Rodriguez, D. R. Evans, R. S. Meltzer, and W. M. Yen, "UV excitation and trapping centers in $CaTiO_3:Pr^{3+}$," J. Lumin. **119–120**, 13–18 (2006).

#180873 - $15.00 USD Received 3 Dec 2012; revised 26 Dec 2012; accepted 7 Jan 2013; published 16 Jan 2013

11. P. Boutinaud, L. Sarakha, E. Cavalli, M. Bettinelli, P. Dorenbos, and R. Mahiou, "About red afterglow in Pr^{3+} doped titanate perovskites," J. Phys. D Appl. Phys. **42**(4), 045106 (2009).
12. X. M. Zhang, J. H. Zhang, Z. G. Nie, M. Y. Wang, X. G. Ren, and X. J. Wang, "Enhanced red phosphorescence in nanosized $CaTiO_3:Pr^{3+}$ phosphors," Appl. Phys. Lett. **90**(15), 151911 (2007).
13. W. Y. Jia, W. L. Xu, I. Rivera, A. Perez, and F. Fernandez, "Effects of compositional phase transitions on luminescence of $Sr_{1-x}Ca_xTiO_3:Pr^{3+}$," Solid State Commun. **126**(3), 153–157 (2003).
14. X. M. Zhang, J. H. Zhang, X. Zhang, L. Chen, Y. S. Luo, and X. J. Wang, "Enhancement of the red emission in $CaTiO_3:Pr^{3+}$ by addition of rare earth oxides," Chem. Phys. Lett. **434**(4–6), 237–240 (2007).
15. S. Y. Yin, D. H. Chen, W. J. Tang, and Y. H. Yuan, "Synthesis of $CaTiO_3$:Pr, Al phosphors by sol-gel method and their luminescence properties," J. Mater. Sci. **42**(8), 2886–2890 (2007).
16. J. F. Tang, X. B. Yu, L. Z. Yang, C. L. Zhou, and X. D. Peng, "Preparation and Al^{3+} enhanced photoluminescence properties of $CaTiO_3:Pr^{3+}$," Mater. Lett. **60**(3), 326–329 (2006).
17. T. Wanjun and C. Donghua, "Photoluminescence properties Pr^{3+} and Bi^{3+}-codoped $CaTiO_3$ phosphor prepared by a peroxide-based route," Mater. Res. Bull. **44**(4), 836–839 (2009).
18. T. Wanjun and C. Donghua, "Photoluminescent properties of $(Ca,Zn)TiO_3:Pr^{3+}$ particles synthesized by the peroxide-based route method," J. Am. Ceram. Soc. **90**(10), 3156–3159 (2007).
19. E. H. Otal, A. E. Maegli, N. Vogel-Schauble, B. Walfort, H. Hagemann, S. Yoon, A. Zeller, and A. Weidenkaff, "The influence of defects formed by Ca excess and thermal post-treatments on the persistent luminescence of $CaTiO_3:Pr^{3+}$," Opt. Mater. Express **2**(4), 405–412 (2012).
20. S. G. Ebbinghaus, H. P. Abicht, R. Dronskowski, T. Muller, A. Reller, and A. Weidenkaff, "Perovskite-related oxynitrides—recent developments in synthesis, characterisation and investigations of physical properties," Prog. Solid State Chem. **37**(2–3), 173–205 (2009).
21. M. H. Yang, J. Oró-Solé, J. A. Rodgers, A. B. Jorge, A. Fuertes, and J. P. Attfield, "Anion order in perovskite oxynitrides," Nat. Chem. **3**(1), 47–52 (2011).
22. A. Maegli, S. Yoon, E. Otal, L. Karvonen, P. Mandaliev, and A. Weidenkaff, "Perovskite-type $SrTi_{1-x}Nb_x(O,N)_3$ compounds: synthesis, crystal structure and optical properties," J. Solid State Chem. **184**(4), 929–936 (2011).
23. A. Fuertes, "Synthesis and properties of functional oxynitrides—from photocatalysts to CMR materials," Dalton Trans. **39**(26), 5942–5948 (2010).
24. J. Rodríguez-Carvajal, "Recent advances in magnetic-structure determination by neutron powder diffraction," Physica B **192**(1–2), 55–69 (1993).
25. A. R. Stokes and A. J. C. Wilson, "The diffraction of x-rays by distorted crystal aggregates," Proc. Phys. Soc. **56**(3), 174–181 (1944).
26. P. Thompson, D. E. Cox, and J. B. Hastings, "Rietveld refinement of Debye-Scherrer synchrotron x-ray data from Al_2O_3," J. Appl. Cryst. **20**(2), 79–83 (1987).
27. T. Ressler, "WinXAS: a program for X-ray absorption spectroscopy data analysis under MS-Windows," J. Synchrotron Radiat. **5**(2), 118–122 (1998).
28. J. A. Bearden and A. F. Burr, "Reevaluation of x-ray atomic energy levels," Rev. Mod. Phys. **39**(1), 125–142 (1967).
29. H. Modrow, "Tuning nanoparticle properties—the x-ray absorption spectroscopic point of view," Appl. Spectrosc. Rev. **39**(2), 183–290 (2004).
30. T. Yamamoto, T. Mizoguchi, and I. Tanaka, "Core-hole effect on dipolar and quadrupolar transitions of $SrTiO_3$ and $BaTiO_3$ at Ti-k edge," Phys. Rev. B **71**(24), 245113 (2005).
31. V. Luca, S. Djajanti, and R. F. Howe, "Structural and electronic properties of sol-gel titanium oxides studied by x-ray absorption spectroscopy," J. Phys. Chem. B **102**(52), 10650–10657 (1998).
32. R. V. Vedrinskii, V. L. Kraizman, A. A. Novakovich, P. V. Demekhin, and S. V. Urazhdin, "Pre-edge fine structure of the 3d atom k x-ray absorption spectra and quantitative atomic structure determinations for ferroelectric perovskite structure crystals," J. Phys. Condens. Matter **10**(42), 9561–9580 (1998).
33. A. I. Frenkel, D. Ehre, V. Lyahovitskaya, L. Kanner, E. Wachtel, and I. Lubomirsky, "Origin of polarity in amorphous $SrTiO_3$," Phys. Rev. Lett. **99**(21), 215502 (2007).
34. T. Hirata, K. Ishioka, and M. Kitajima, "Vibrational spectroscopy and x-ray diffraction of perovskite compounds $Sr_{1-x}M_xTiO_3$ (M= Ca, Mg; $0 \le x \le 1$)," J. Solid State Chem. **124**(2), 353–359 (1996).
35. H. Zheng, H. Bagshaw, G. D. C. Csete de Györgyfalva, I. M. Reaney, R. Ubic, and J. Yarwood, "Raman spectroscopy and microwave properties of $CaTiO_3$-based ceramics," J. Appl. Phys. **94**(5), 2948–2956 (2003).
36. V. S. Marques, L. S. Cavalcante, J. C. Sczancoski, D. P. Volanti, J. W. M. Espinosa, M. R. Joya, M. R. M. C. Santos, P. S. Pizani, J. A. Varela, and E. Longo, "Influence of microwave energy on structural and photoluminescent behavior of $CaTiO_3$ powders," Solid State Sci. **10**(8), 1056–1061 (2008).
37. U. Balachandran and N. G. Eror, "Laser-induced Raman-scattering in calcium titanate," Solid State Commun. **44**(6), 815–818 (1982).
38. M. Stachiotti, A. Dobry, R. Migoni, and A. Bussmann-Holder, "Crossover from a displacive to an order-disorder transition in the nonlinear-polarizability model," Phys. Rev. B Condens. Matter **47**(5), 2473–2479 (1993).
39. A. Bussmann-Holder, A. R. Bishop, and G. Benedek, "Quasiharmonic periodic traveling-wave solutions in anharmonic potentials," Phys. Rev. B **53**(17), 11521–11530 (1996).
40. E. A. Stern, "Character of order-disorder and displacive components in barium titanate," Phys. Rev. Lett. **93**(3), 037601 (2004).
41. P. Boutinaud, E. Pinel, M. Dubois, A. P. Vink, and R. Mahiou, "UV-to-red relaxation pathways in $CaTiO_3:Pr^{3+}$," J. Lumin. **111**(1–2), 69–80 (2005).

#180873 - $15.00 USD Received 3 Dec 2012; revised 26 Dec 2012; accepted 7 Jan 2013; published 16 Jan 2013

42. K. Maeda, H. Terashima, K. Kase, M. Higashi, M. Tabata, and K. Domen, "Surface modification of taon with monoclinic ZrO_2 to produce a composite photocatalyst with enhanced hydrogen evolution activity under visible light," Bull. Chem. Soc. Jpn. **81**(8), 927–937 (2008).
43. V. N. Kuznetsov and N. Serpone, "On the origin of the spectral bands in the visible absorption spectra of visible-light-active TiO_2 specimens analysis and assignments," J. Phys. Chem. C **113**(34), 15110–15123 (2009).
44. A. Zhu, J. Wang, D. Zhao, and Y. Du, "Native defects and Pr impurities in orthorhombic $CaTiO_3$ by first-principles calculations," Physica B **406**(13), 2697–2702 (2011).
45. N. J. Cockroft and J. C. Wright, "Local- and distant-charge compensation of Eu^{3+} ions in defect centers of $SrTiO_3$," Phys. Rev. B **45**(17), 9642–9655 (1992).
46. R. Fujiwara, H. Sano, M. Shimizu, and M. Kuwabara, "Quantitative analysis of uv excitation bands for red emissions in Pr^{3+}-doped $CaTiO_3$, $SrTiO_3$ and $BaTiO_3$ phosphors by peak fitting," J. Lumin. **129**(3), 231–237 (2009).
47. X. M. Zhang, C. Y. Cao, C. H. Zhang, L. Chen, J. H. Jia, and X. J. Wang, "Improved photoluminescence and afterglow in $CaTiO_3$:Pr^{3+} with addition of nanosized SiO_2," Physica B **406**(20), 3891–3895 (2011).
48. X. M. Zhang, C. Y. Cao, C. H. Zhang, S. Y. Xie, G. W. Xu, J. H. Zhang, and X. J. Wang, "Photoluminescence and energy storage traps in $CatiO_3$:Pr^{3+}," Mater. Res. Bull. **45**(12), 1832–1836 (2010).

1. Introduction

Solid-state non-candescent light sources such as white light-emitting diodes (LED) are an emerging technology due to the enhanced performances and energy efficiencies well beyond those of traditional artificial lighting [1]. Over the past few decades considerable efforts have been spent on the development of new phosphors to meet the color quality and efficiency required for solid-state lighting. For example, the green-luminescent $SrAl_2O_4$:Eu^{2+}/Dy^{3+} phosphor with a strong emission at 520 nm has been extensively studied and applied, since it was first reported by Matsuzawa *et al.* [2]. The $Sr_4Al_{14}O_{25}$:Eu^{2+}/Dy^{3+} phosphor was developed in the mid-1990s showing extremely prolonged blue-green phosphorescence (495 nm) that lasts over 20 hours [3,4]. These green and blue phosphors based on strontium aluminate are attractive options due to their long afterglow, chemical stability and high quantum yield [5], which allow for various applications for these materials such as luminescent paint, safety illumination and emergency lighting. As such, the development of novel red-emitting phosphors is especially required to complete the color spectrum. Many efforts are currently undertaken not only to synthesize new phosphors but also to improve the luminescence properties of already discovered red-emitting phosphors.

Since the red emission of Pr^{3+}-doped $CaTiO_3$ was reported [6,7], the development of the $CaTiO_3$:Pr^{3+} phosphor especially for display and lighting technologies has been highly promoted [8]. The mechanism of the persistent luminescence of $CaTiO_3$:Pr^{3+} is well understood [7,9–11]. Ultraviolet light irradiation on $CaTiO_3$:Pr^{3+} phosphor creates electron–hole pairs in conduction and valence bands of the host $CaTiO_3$. These charge carriers can be mainly stabilized by trapping centers such as oxygen vacancies. Afterglow was then attributed to thermal activation of electrons stored in the trapping centers following the red emissions peaking at 612 nm due to the $^1D_2 \rightarrow {}^3H_4$ transition of Pr^{3+}. Thus the presence of oxygen vacancies or associations of oxygen vacancies is known to be essential for the red phosphorescence with long afterglow time [12,13]. Additionally, for the improved photoluminescence and afterglow in $CaTiO_3$:Pr^{3+}, more electron–hole pairs should be transferred from the host $CaTiO_3$ to the luminescence center Pr^{3+} without recombination process on non-radiative recombination centers. According to Zhang *et al.* [14], negatively charged Ca and Ti vacancies are found to be the main crystal defects in $CaTiO_3$:Pr^{3+} phosphors to compensate the extra positive charge of Pr^{3+}, which act as non-radiative recombination centers reducing the fluorescence emission efficiency.

Great efforts have been made to improve the optical performance including the excitation/emission intensity and the afterglow (phosphorescence decay profile). With respect to these findings different approaches, for example, the synthesis methods, the co-dopants, the host modifications or the particle size have been pursued. Yin *et al.* reported that phosphors synthesized by the sol-gel method outperformed those prepared using the solid-state approach [15]. Zhang *et al.* reported that nanosized $CaTiO_3$:Pr^{3+} phosphors exhibited stronger and longer phosphorescence than the bulk samples [12]. In addition to Al^{3+} or Bi^{3+} [16,17], Zn^{2+} and/or B^{3+} substitution [8,18] have been found to intensify the red emission of $CaTiO_3$:Pr^{3+}.

#180873 - $15.00 USD Received 3 Dec 2012; revised 26 Dec 2012; accepted 7 Jan 2013; published 16 Jan 2013

Recently, the influence of defects in $CaTiO_3:Pr^{3+}$ generated by cation substitution have been investigated. Adding 3% Ca excess followed by thermal treatment at 1400 °C results in afterglow improvement [19]. The influence of anionic defects which can be affected by an ammonia treatment, however, has not been investigated so far. The decomposition of ammonia at high temperature leads to active nitriding gases and molecular hydrogen. Thus thermal ammonolysis is commonly used for the reduction or nitridation of oxide precursors [20–23].

In the present study, $CaTiO_3:Pr^{3+}$ powders were synthesized by a solid state reaction and treated with NH_3 at different temperatures. The influence of thermal ammonolysis on the long- and short-range order of the crystal structure was investigated by X-ray diffraction, X-ray absorption spectroscopy and Raman spectroscopy. The resulting afterglow decay curves have been studied by fluorescence spectrophotometry. The correlation between the defects and the luminescence properties is discussed.

2. Experimental section

$CaTiO_3:Pr^{3+}$ powders with the nominal composition $Ca_{0.998}Pr_{0.002}TiO_{3-\delta}$ were repeatedly synthesized by a solid-state reaction. Stoichiometric amounts of $CaCO_3$ (Riedel-de Haën, ≥ 98.5%) and TiO_2 (Sigma- Aldrich, ≥ 98.5%) along with 0.2 mol % of Pr_2O_3 (Alfa Aesar, 99.9%) were ground in a planetary ball mill using ZrO_2 balls and ethanol and dried at 100 °C. The well ground powders were then calcined at 1500 °C for 24 h in air to obtain single phase Pr-doped $CaTiO_3$. The obtained $CaTiO_3:Pr^{3+}$ powder will be denoted in the following as CTO-pristine. Separately, aliquots of the powders were calcined at 1300 and 1400 °C in order to check the effect on the photoluminescence excitation spectra.

The thermal ammonolysis was carried out in a rotating cavity reactor. Roughly 3 g CTO-pristine were heated at 300, 400, 500, and 600 °C under 35 mL/min NH_3 (Messer, ≥ 99.99%). In the following these samples are denoted as NH_3-300C, NH_3-400C, NH_3-500C, NH_3-600C, respectively. The reaction was terminated after 2.5 h by quenching the ammonolyzed samples to room temperature in NH_3 atmosphere.

Powder X-ray diffraction patterns were obtained using a PANalytical X´Pert PRO θ-2θ scan system equipped with a Johansson monochromator (Cu-$K\alpha_1$ radiation, 1.5406 Å) and an X'Celerator linear detector. The diffraction patterns were recorded between 20° and 100° (2θ) with an angular step interval of 0.0167°. Lattice parameters, strain and bond lengths/angles were determined by Rietveld refinement using the program *FullProf* [24]. The calculated strain corresponds to 1/4 of the strain derived from the Stokes and Wilson expression [25]. The Thompson-Cox-Hastings pseudo-Voigt function [26] was used as profile function and CeO_2 (NIST SRM674b) was measured as standard reference material in order to estimate the device-specific contribution to the peak broadening.

Ti *K*-edge X-ray absorption spectra (XAS) were measured at beamline A1 of HASYLAB at DESY (Hamburg, Germany). The incident X-ray beam was energy-resolved using a Si(111) double crystal monochromator. Higher-order harmonic contributions were eliminated by detuning the monochromator. Higher order harmonic contributions were eliminated by detuning the monochromator to 60% of the maximum energy. The spectra were collected in transmission mode at room temperature. The obtained XANES spectra were processed using the program *WinXAS* [27]. The background correction was performed by two fits in the energy ranges 4.766 – 4.966 keV and 5.030 – 6.260 keV with first- and second-order polynomial functions, respectively. The spectra were normalized using the energy range 5.030 – 5.200 keV. The photon energy of XAS spectra was calibrated with the first inflection point of a titanium metal foil reference, which was assigned to 4.966 keV [28].

Raman spectra were recorded using a Renishaw 2000 spectrometer equipped with holographic notch filters for elastic scattering and a CCD array detector. The samples were excited with a red He-Ne laser (632.816 nm). The laser was focused onto the sample using the objective lenses (20 × magnification). The instrumental setup was calibrated with a Si single crystal. The spectra were recorded at room temperature with an exposure time of 10 s. The measurement was repeated five times and accumulated.

#180873 - $15.00 USD Received 3 Dec 2012; revised 26 Dec 2012; accepted 7 Jan 2013; published 16 Jan 2013

Thermogravimetric analysis (TGA) was carried out using a NETZSCH STA 409 CD thermobalance. A baseline was measured with empty crucible and then about 0.1 g of the sample powders were heated in alumina crucibles applying a heating rate of 10 °C/min up to 1500 °C in synthetic air (50 mL/min). Luminescence spectra were obtained using a Jobin Yvon Fluorolog 3-22 instrument with a nominal resolution ranging from 0.5 to 2 nm. Low temperature experiments were realized with a Janis closed cycle cryostat.

Phosphorescence decay profiles have been measured with a home-made photometer (Phototec, developed by RC Tritec in collaboration with Monyco) equipped with a high sensitive photomultiplier from Hamamatsu. The spectra were recorded after excitation by 6 UV-LED in very short distance for one minute to fully activate the phosphors.

UV-visible diffuse reflectance spectra were acquired using a UV–3600 Shimadzu UV–VIS NIR spectrophotometer equipped with an integrating sphere. The baseline measurement was taken with $BaSO_4$. The spectra were recorded in the range of 200 – 1200 nm.

3. Results and discussion

X-ray diffraction patterns of $CaTiO_3:Pr^{3+}$ powders are shown in Fig. 1. All reflections observed correspond to an orthorhombic crystal structure (JCPDS-PDF No. 01-082-0228, space group: *Pbnm*) and no diffraction peaks arising from secondary phases or impurities are found. This suggests that during the thermal ammonolysis no detectable side reaction or phase decomposition occurred preserving the structure. Figure 2 presents the selected XRD pattern and Rietveld plot of NH_3-400C. The refinement results of the cell parameters together with the reliability factors of all five samples are given in Table 1. The unit-cell volume of NH_3-400C was smallest among all samples. Moreover, the smallest lattice strain was obtained for NH_3-400C. Based on the atomic positions in the unit-cell obtained by Rietveld refinement, bond lengths and angles are calculated and summarized in Table 2. Interestingly, NH_3-400C exhibits the shortest average Ti-O bond length and the largest average Ti-O-Ti angle.

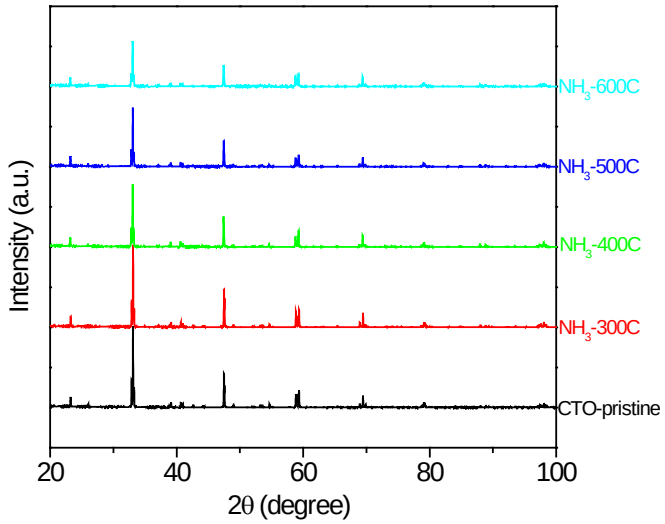

Fig. 1. Powder X-ray diffraction patterns of $CaTiO_3:Pr^{3+}$ ammonolyzed at different temperatures.

#180873 - $15.00 USD Received 3 Dec 2012; revised 26 Dec 2012; accepted 7 Jan 2013; published 16 Jan 2013

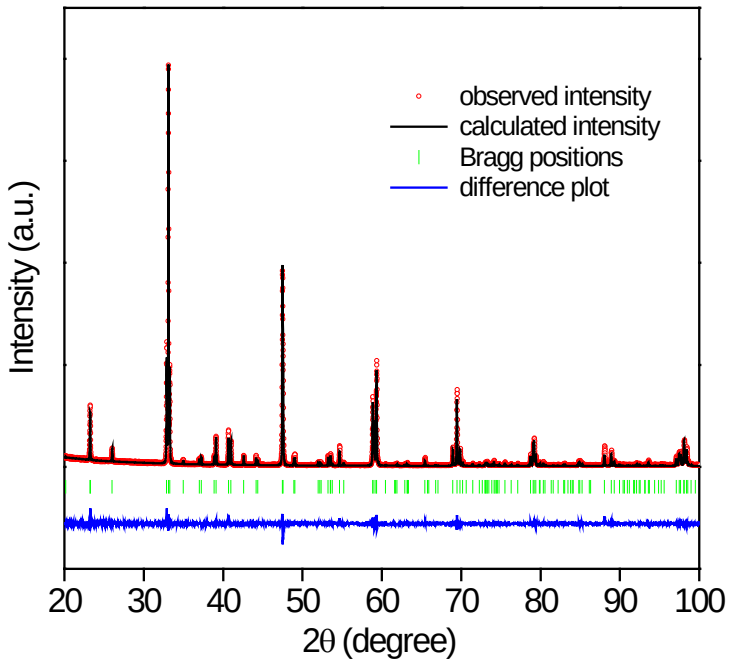

Fig. 2. XRD pattern and Rietveld refinement of $CaTiO_3:Pr^{3+}$ ammonolyzed at 400 °C. The difference plot of observed and calculated diffraction profiles is shown together with the Bragg positions (short vertical markers).

Table 1. Rietveld Refinement Results of All $CaTiO_3:Pr^{3+}$ Samples

Sample		CTO-pristine	NH_3-300C	NH_3-400C	NH_3-500C	NH_3-600C
Lattice parameter (Å)	*a*	5.38163(3)	5.38231(3)	5.38136(3)	5.38219(4)	5.38193(2)
	b	5.44386(3)	5.44446(3)	5.44351(3)	5.44464(4)	5.44418(2)
	c	7.64316(4)	7.64383(4)	7.64260(5)	7.64380(6)	7.64344(3)
Unit-cell volume ($Å^3$)		223.921(2)	223.993(2)	223.879(2)	223.994(3)	223.954(2)
Lattice strain ($\times 10^{-4}$)		3.5481	4.2508	3.1515	4.9697	5.1091
R_p (%)		8.93	9.01	8.64	9.33	6.79
R_{wp} (%)		12.5	12.8	12.6	13.0	8.67
R_{exp} (%)		7.65	7.56	7.82	8.02	5.91
χ^2		2.66	2.85	2.60	2.61	2.15

Space group symmetry: *P b n m*
R_p, R_{wp}, R_{exp}, and χ^2 are the reliability factors and goodness-of-fit, respectively.
Numbers in parentheses are the estimated standard deviation.

Table 2. Selected Bond Lengths (Å) and Angles (°) in $CaTiO_3:Pr^{3+}$

Sample	CTO-pristine	NH_3-300C	NH_3-400C	NH_3-500C	NH_3-600C
$<Ti\text{-}O>_{length}$ [a]	1.960	1.957	1.955	1.955	1.956
$<Ca\text{-}O>_{length}$ [b]	2.734	2.728	2.726	2.727	2.727
$<Ti\text{-}O\text{-}Ti>_{angle}$ [c]	154.898	155.735	156.182	156.132	155.913

[a]The average length calculated with the 6 shortest bond lengths.
[b]The average length calculated with the 12 shortest bond lengths.
[c]The average angle calculated with the 6 bond angles.

The pre-edge regions of the normalized Ti *K*-edge XANES spectra are shown in Fig. 3. XANES is not only a subtle probe of the chemical environment of the elements but it is also highly sensitive to the local structure around X-ray absorbing atoms [29]. The pre-edge peak features changed with the ammonolysis temperature and in turn with the variation of the

#180873 - $15.00 USD Received 3 Dec 2012; revised 26 Dec 2012; accepted 7 Jan 2013; published 16 Jan 2013

anionic sublattice of $CaTiO_3$, evidencing local structural changes around the Ti ion. The physical origin of the pre-edge feature A_1 is still debated, a core-hole effect coupled with the dipolar and quadrupolar transitions [30] or 3*d*-4*p* hybridized states [31] being the most plausible explanations. The strong A_2 and A_3 features originate from the transition of the 1*s* electron to an unfilled 3*d* state. This dipole forbidden transition becomes allowed by the mixing of 2*p* states of the surrounding oxygen atoms into the 3*d* states of titanium atoms due to a non-centrosymmetric distortion of the octahedral TiO_6 polyhedron [32,33]. Therefore, the A_2 and A_3 features are interpreted as indicators for the displacement of Ti ions from the center of the TiO_6 octahedron. The XANES spectra of ammonolyzed powders show no noticeable change in any of the pre-edge peak intensities. However, the A_2 and A_3 features of CTO-pristine show the highest intensities indicating the largest off-center displacement. Thus, a highly off-centered, in other words distorted, TiO_6 octahedron was confirmed for CTO-pristine by XANES.

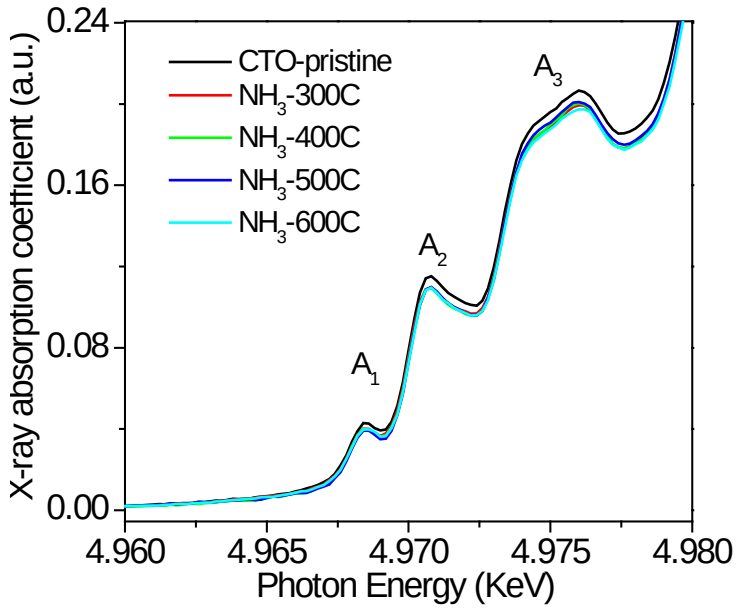

Fig. 3. Ti *K*-edge XANES spectra of the pre-edge region of $CaTiO_3:Pr^{3+}$ ammonolyzed at different temperatures.

Figure 4(a) shows the Raman spectra. Seven Raman modes in the wavenumber range 200 to 800 cm^{-1} can be attributed to the orthorhombic crystal structure, in good agreement with the XRD results and literature [34–36]. Raman active modes changed as a function of the ammonolysis temperatures indicating changes in the local structure. For instance, the Raman signal at 641 cm^{-1} is assigned to the symmetric stretching vibration of the Ti-O bond [35,37]. Noticeable increase in intensity of signal was observed for NH_3-400C as compared to the other samples. This indicates that thermal ammonolysis at 400 °C leads to an enhanced local symmetry at the Ti center (Fig. 4(b)). This is in agreement with the XRD data that show the smaller lattice strain for NH_3-400C than for the other samples. However, XANES pre-edge features of all ammonolyzed powders nearly coincide suggesting that the local structure around the Ti cation in the TiO_6 octahedron remained unchanged. The seemingly contradictory results of XANES and Raman spectroscopy might be due to the different averaging time scales of the measuring techniques [38,39]. In this study, Raman spectroscopy averages collective dynamic displacements in times of the order of 10^{-10} seconds or longer. On the other hand, XAS has an averaging time of less than 10^{-15} s [40]. Thus, XAS measures the instantaneous displacement of the atoms and Raman spectroscopy measures the changes

#180873 - $15.00 USD Received 3 Dec 2012; revised 26 Dec 2012; accepted 7 Jan 2013; published 16 Jan 2013

of atom position after much longer times. Another possible explanation for our observation can be given by the sensitivity of measurement techniques, indicating that the Raman spectroscopy is much more sensitive to the subtle changes of vibration modes and thus local symmetry breaking and distortion around TiO_6 than XAS.

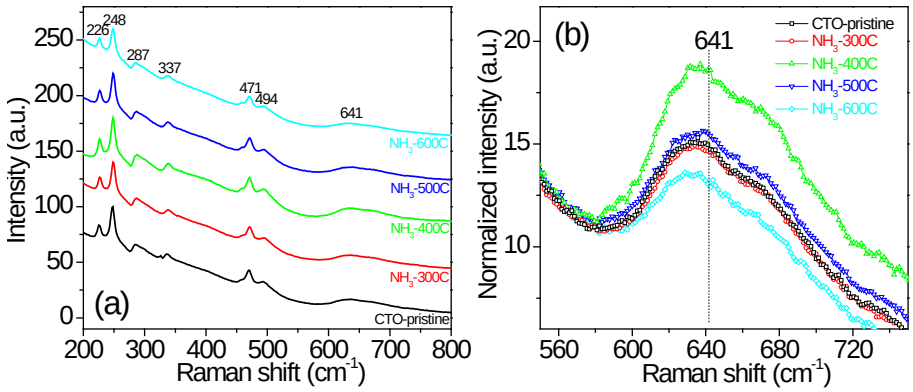

Fig. 4. (a) Raman spectra of $CaTiO_3:Pr^{3+}$ powders measured at room temperature, (b) 550 – 750 cm^{-1} regions enlarged.

Figure 5 illustrates the mass changes during thermogravimetric analysis (TGA) in synthetic air. CTO-pristine showed the largest and NH_3-400C the smallest mass loss of *ca.* 0.4% and 0.04%, respectively. The mass loss was mainly attributed to the release of oxygen in $CaTiO_3$ at high temperature. Therefore, it can be concluded that NH_3-400C was least reduced during the re-oxidation study.

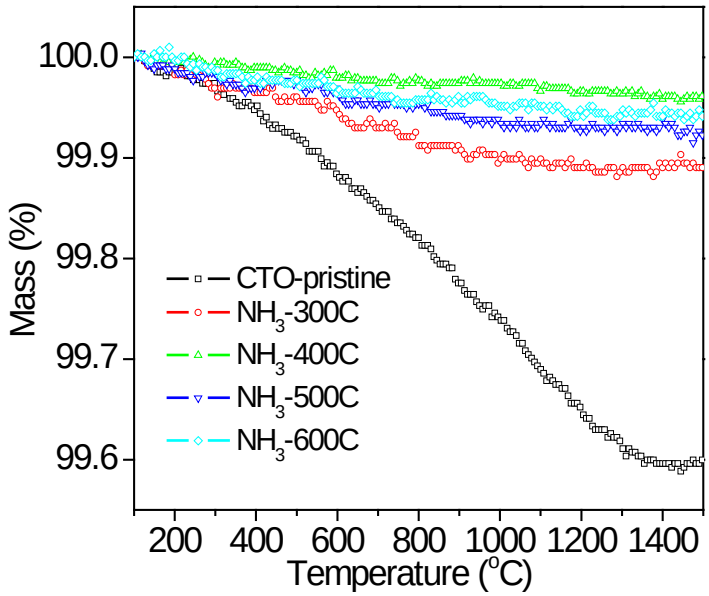

Fig. 5. Thermogravimetric analysis (TGA) of $CaTiO_3:Pr^{3+}$ ammonolyzed at different temperatures.

Figure 6 compares room temperature excitation spectra (λ = 612 nm) of $CaTiO_3:Pr^{3+}$ (0.2%) synthesized by the solid-state reaction and annealed 24 h in air at 1300, 1400 and 1500 °C. The band at roughly 330 nm was attributed to the bandgap excitation of the $CaTiO_3$ host (the valence to conduction band transition) [7]. At lower energies, the band at 370 nm was

#180873 - $15.00 USD Received 3 Dec 2012; revised 26 Dec 2012; accepted 7 Jan 2013; published 16 Jan 2013

assigned to a charge transfer between Pr^{3+} and Ti^{4+} [41], and at higher energies (between 200 and 300 nm), the 4*f* to 5*d* excitation of Pr^{3+} is assigned. The weak excitation bands between 450 and 500 nm correspond to $^3H_4$ to $^1I_6$ and $^3H_4$ to ^3P_J (J = 0, 1, 2) transitions of Pr^{3+} (inset in Fig. 6). It is supposed that Pr^{3+} is located on the Ca^{2+} site. This requires that the different charge must be compensated somehow. The sample annealed at 1400 °C showed the simplest spectrum, with a maximum at 330 nm and a broad shoulder at roughly 280 nm in addition to the bands at lower energy. The sample annealed at 1500 °C reveals an additional broad component centered at 295 nm, while the sample annealed at 1300 °C reveals another sharp excitation band at 312 nm. When $CaTiO_3$: Pr^{3+} powder was annealed separately at 1500 °C in a different Al_2O_3 crucible, the relative intensity of the band at 370 nm has become roughly 5 times stronger than all the other samples. It is not yet clear why the band at 370 nm shows different intensity depending on the used crucible. One possible reason might be the oxygen deficiencies. Depending on the shape and volume of Al_2O_3 crucible, the amount of powders exposed to the surface is different and as a result, different degrees of surface oxidation are anticipated. Though the crucibles are cleaned in order to avoid contamination from previous use, we cannot exclude the possible contamination with Cr^{3+} impurity, which is commonly contained in alumina crucible. For the NH_3-treated samples, the spectra measured at 5K (Fig. 7) show an additional contribution to the band at 370 nm (red-shifted by 5 nm). We have also observed previously [19] that Ca-excess significantly contributes to the intensity of the band at 370 nm. As this band corresponds to a charge transfer between Pr^{3+} and Ti^{4+} in the crystal, the overall findings indicate that the concentration and the distribution of Pr^{3+} and Ti^{4+} was indeed affected by the NH_3-treatment.

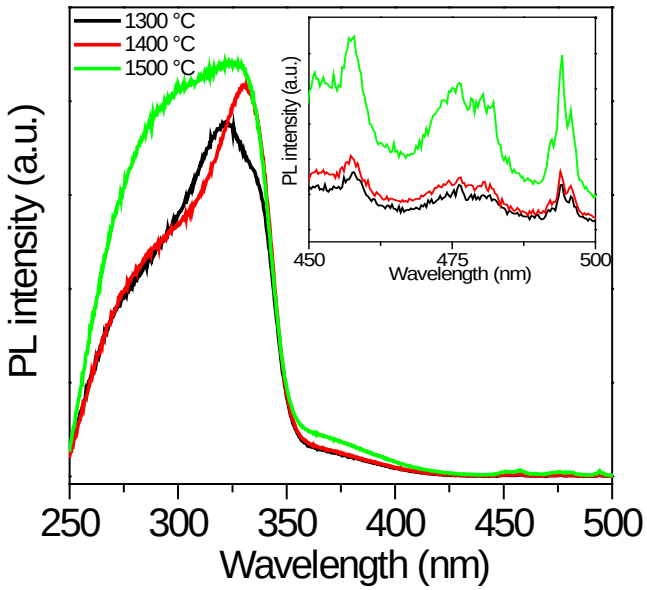

Fig. 6. Photoluminescence excitation spectra ($\lambda_{emission}$ = 612 nm) measured at 294 K in air for the samples annealed at 1300 °C, 1400 °C and 1500 °C. The inset shows the enlarged 450 – 500 cm^{-1} regions.

#180873 - $15.00 USD Received 3 Dec 2012; revised 26 Dec 2012; accepted 7 Jan 2013; published 16 Jan 2013

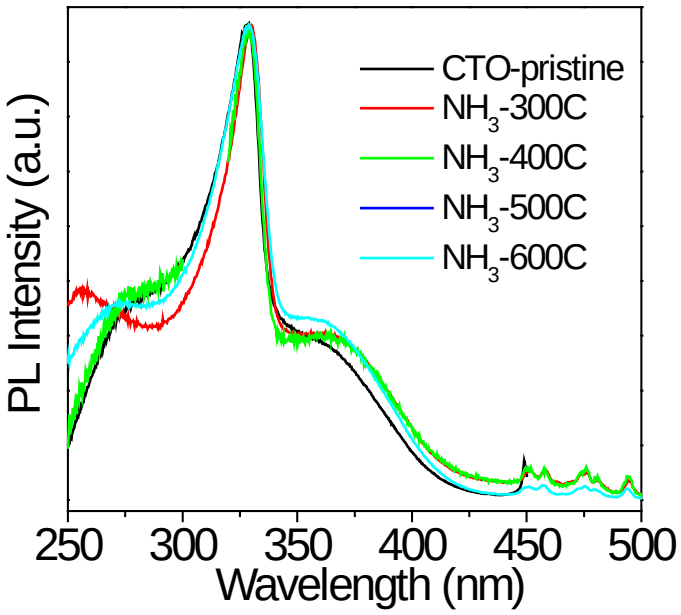

Fig. 7. Photoluminescence excitation spectra ($\lambda_{emission}$ = 612 nm) for $CaTiO_3:Pr^{3+}$ measured at 5 K. The excitation spectra are normalized by the peak intensity at 330 nm.

Temperature dependent excitation spectra from 5 K to 300 K (Fig. 8) revealed a significant broadening of the sharp *f-f* bands (between 450 and 500 nm) upon heating. The 330 nm band also broadens significantly, and the relative intensity of the 280 nm band increases. This increase of intensity could be related to an improved Frank-Condon contribution (by the population of excited vibrational levels in the electronic ground state) of the *f-d* absorption of the Pr^{3+} ion.

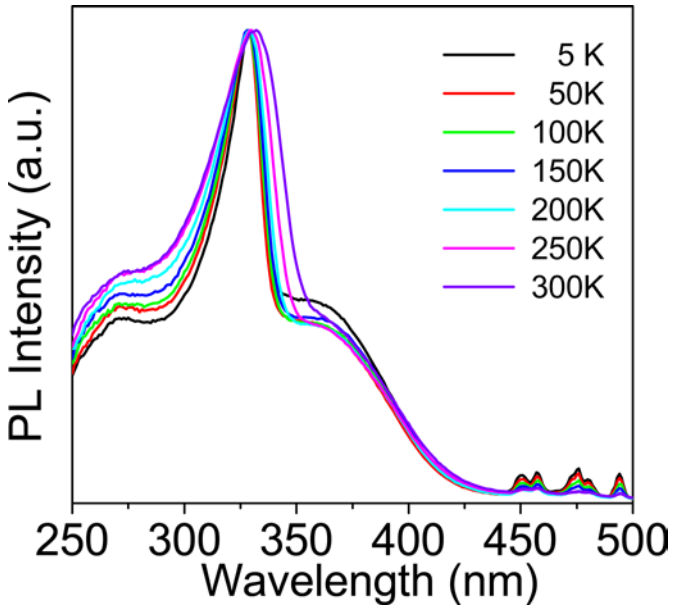

Fig. 8. Photoluminescence excitation spectra ($\lambda_{emission}$ = 612 nm) for NH_3-400C at 5 K, 50 K, 100 K, 150 K,200 K, 250 K and 300 K. The excitation spectra are normalized by the peak intensity at 330 nm.

#180873 - $15.00 USD Received 3 Dec 2012; revised 26 Dec 2012; accepted 7 Jan 2013; published 16 Jan 2013

Figure 9 illustrates the phosphorescence decay profiles of all samples. It is found that the phosphorescence intensities of NH_3-300C and NH_3-400C are higher compared to CTO-pristine but decrease again with further increasing ammonolysis temperature. Thus, the highest phosphorescence intensity is observed for NH_3-400C.

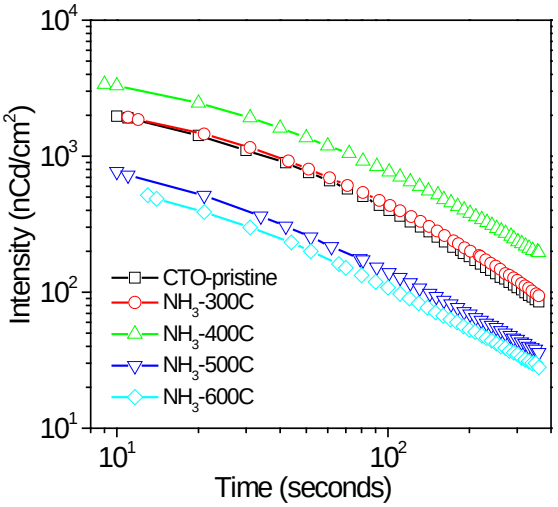

Fig. 9. Phosphorescence decay profiles of $CaTiO_3:Pr^{3+}$ phosphors.

Figure 10 shows UV-Vis diffuse reflectance spectra as a function of wavelength. NH_3 treatment did not lead to a shift of the absorption edge indicating that the bandgap energy of the samples was not affected. The determined absorption edge wavelength of roughly 330 nm is in agreement with the photoluminescence excitation spectroscopy results (Fig. 8). While the intensities did not change in the UV region below the absorption edge, an increase was observed in the wavelength range of 400 nm to 900 nm with NH_3-400C showing the highest reflectance. The color of the powders changed from grayish-white for CTO-pristine to bright white for NH_3-400C. An increase of the UV-Vis reflectance above the bandgap wavelength can be interpreted as a reduction of the defect concentration [42,43]. Thus, UV-Vis spectroscopy revealed that the increase of the phosphorescence intensity (Fig. 10) is correlated with the decrease of the defect concentration.

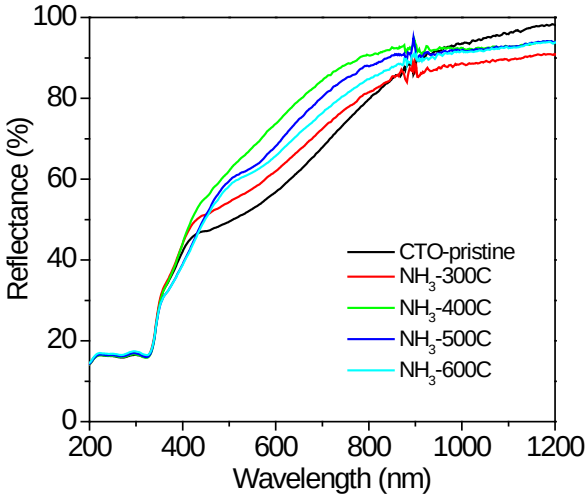

Fig. 10. UV-Vis diffuse reflectance spectra of $CaTiO_3:Pr^{3+}$ powders ammonolyzed at different temperatures.

#180873 - $15.00 USD Received 3 Dec 2012; revised 26 Dec 2012; accepted 7 Jan 2013; published 16 Jan 2013

As already mentioned, the luminescence properties depend strongly on the defect states and this is why the defects chemistry is discussed below. In this study, Pr^{3+} was added into the $CaTiO_3$ lattice as a luminescence center with the nominal composition $Ca_{0.998}Pr_{0.002}TiO_{3-\delta}$. To compensate the extra positive charge of Pr^{3+} in Ca site, mainly two possible defect reactions can be formulated. First, negatively charged Ca and Ti vacancies which act as non-radiative recombination centers can be formed [14,44]. Secondly, the incorporated Pr^{3+} can be accompanied by generation of excess oxygen and/or reduction of the oxygen vacancies to compensate the extra positive charge. Defects formed by excess oxygen also act as non-radiative recombination centers hampering the process of energy transfer from the host to Pr^{3+}. In this study, much interest has been focused on the excess oxygen because enhanced photoluminescence properties cannot be explained by the change of Ca and Ti vacancies during the NH_3 treatment. Rather, excess oxygen can be controlled by the reducing NH_3 treatment. In addition, we cannot rule out the possibility that Pr^4 is reduced to Pr^{3+} by the NH_3 treatment. NH_3 plays a role as a reducing and a nitriding agent during the thermal treatment [20,22,23]. Whether the reduction or nitridation reaction is dominant depends on the compounds and reaction conditions. In this study, however, thermal ammonolysis between 300 and 500 °C did not lead to nitrogen incorporation into the lattice, which was confirmed by hot-gas extraction (data not shown here). In the given temperature range the powders were primarily reduced. In order to verify the reducing effect of NH_3 in $CaTiO_3:Pr^{3+}$ phosphors CTO-pristine sample was annealed in flowing air (10 mL/min) at 1000 °C for 12 h, which deteriorated the photoluminescence intensity and reduced the UV-Vis reflectance compared to the CTO-pristine sample (data not shown here). Reduced unit-cell volume and lattice strain as well as the enhanced local symmetry of NH_3-400C imply that the NH_3 treatment actually led to the removal of interstitial oxygen originally incorporated in the as-synthesized $CaTiO_3:Pr^{3+}$. This is also consistent with the TGA result of NH_3-400C that shows the smallest mass loss because the mass loss is attributed to the release of oxygen. As a result, enhanced photoluminescence, increased phosphorescence intensity and the highest UV-Vis reflectance is obtained for NH_3-400C due to the minimized defect concentration and strain. It is well known that perovskite-type oxides tend to have significant amounts of point defects, when they are synthesized at high temperature in air [45]. In general, the photoluminescence efficiency is sensitive to the symmetry and strength of the crystal field [46]. Therefore, the influence of NH_3 treatment can be described as regulation of the crystal structure by reducing the concentration of defects which act as non-radiative recombination centers, and by simultaneous release of the lattice strain. However, the generation of oxygen vacancies due to $CaTiO_3$ reduction and the reduction of Pr^{4+} to Pr^{3+} during the ammonolysis cannot be ruled out because a certain amount of oxygen vacancies and increased amount of Pr^{3+} is beneficial for the luminescence properties [46–48]. Electron paramagnetic resonance (EPR) spectroscopy or thermoluminescence spectroscopy could shed light on this topic.

4. Conclusions

$CaTiO_3:Pr^{3+}$ phosphors were treated under flowing NH_3 at different temperatures. By Rietveld refinements, the smallest lattice strain was identified for the sample annealed at 400 °C. Raman spectroscopy revealed that NH_3-400C also has the highest local (short-range) symmetry of all samples. Increased phosphorescence decay profiles associated with the highest UV-Vis reflectance for the powders ammonolyzed at 400 °C was attributed to the reduced concentration of interstitial oxygen and enhanced degree of order of the crystal structure.

Acknowledgments

The authors are also grateful to Mr. Bartosz Penkala for his support with the UV-Vis spectroscopy. Part of this research was carried out at the synchrotron DORIS III at DESY, a member of the Helmholtz Association (HGF). We would like to thank Dr. Edmund Welter for his assistance. The Commission for Technology and Innovation (CTI) is gratefully acknowledged for financial support (project number, 10640.1;3 PFIW-IW).

#180873 - $15.00 USD Received 3 Dec 2012; revised 26 Dec 2012; accepted 7 Jan 2013; published 16 Jan 2013